Construction and Building Materials 171 (2018) 232–242

Contents lists available at ScienceDirect

Construction and Building Materials

journal homepage: www.elsevier.com/locate/conbuildmat

Effect of pore structure on the performance of photocatalytic lightweight lime-based finishing mortar

C. Giosuè [a,*], Q.L. Yu [b,*], M.L. Ruello [a], F. Tittarelli [a,c], H.J.H. Brouwers [b]

[a] Department of Materials, Environmental Sciences and Urban Planning – SIMAU, Università Politecnica delle Marche, UdR INSTM, 60131 Ancona, Italy
[b] Department of the Built Environment, Eindhoven University of Technology, P.O. Box 513, 5600 MB Eindhoven, The Netherlands
[c] ISAC-CNR Bologna, Italy

HIGHLIGHTS

- Photocatalytic lightweight indoor hydraulic lime-based finishing mortar is designed.
- Effect of expanded glass and expanded silicate on photocatalytic activity is assessed.
- Effect of pore structure of lightweight mortar on photocatalytic activity is studied.
- Drying shrinkage and water absorption of the lightweight finishing mortar are studied.
- Thermal properties of the lightweight finishing mortar are studied.

ARTICLE INFO

Article history:
Received 13 July 2017
Received in revised form 17 February 2018
Accepted 13 March 2018

Keywords:
Lightweight mortar
Pore structure
Compressive strength
Drying shrinkage
Indoor Air Quality
Photocatalytic oxidation
Capillary water absorption

ABSTRACT

The present paper aims to evaluate the performance of photocatalytic lightweight indoor hydraulic lime-based finishing mortars, with Portland cement-based finishing mortar as a reference. Two different types of aggregates, expanded glass and expanded silicate, are utilized to achieve the lightweight character and their contributions are investigated. The pore structure of the developed mortars is determined by mercury intrusion porosimetry (MIP) and BET methods. The mechanical strength, drying shrinkage, thermal physical properties and air pollutant removal ability of the mortars are investigated and the effects of pore structure on these properties are evaluated.

Due to the higher porosity, lime-based finishing mortars possess a higher capillary water absorption and higher drying shrinkage, which can be explained by the Kelvin-Laplace mechanism. The lime-based mortar shows very good thermal properties, with a thermal conductivity of 0.15 W/(m·K). The lime-based mortar shows a better ability of removing air pollutants, up to 46% under indoor air conditions laboratory test, compared to the cement-based mortar, which is attributed to the lower content of gel pores present in the lime-based mortar. Expanded glass shows positive influences concerning thermal properties and air pollutant removal ability compared to expanded silicate.

1. Introduction

The construction sector is a major energy consumer, contributing to 40% of the global emissions of CO_2 [1], taking into account all aspects from transports and production of materials to all the active engineered systems that operate in buildings. This prompts engineers, architects and researchers to carefully choose construction materials for designing and to build better sealed constructions in order to reduce the thermal loss. In this perspective, if sufficient air change is not guaranteed, air pollutants in building environments can reach a harmful level for human health. Indoor Air Quality (IAQ) has received great attention in the last few years because people spend about 90% of time indoors [2]. The design and construction of a high air-tight indoor environments without providing an adequate ventilation system can cause insufficient air renewal with a consequent increase in concentration of pollutants, which could be higher than outdoors [3,4]. Traditional methods are not suitable to solve the problem, as sometimes it is not possible to reduce the source emission or the use of active systems that increase the energy demand of the building.

Heterogeneous photocatalytic oxidation (PCO) represents a promising option to ensure a healthier indoor environment [5] without additional energy costs. PCO is superficial phenomena

* Corresponding authors.
E-mail addresses: c.giosue@univpm.it (C. Giosuè), q.yu@bwk.tue.nl (Q.L. Yu).

https://doi.org/10.1016/j.conbuildmat.2018.03.106
0950-0618/

[6,7], and the process has been extensively studied previously [8]. Nowadays there is an increasing interest in applying this principle in cementitious materials [9] and the study of synergetic use of pre-activation techniques and modification with nano-silica [10] or transition metal ions [11]. Those efforts have been devoted to developing indoor material with the addition of a photocatalytic agent either in bulk or as coating [12–15]. The essence of the research strategy to solve this problem is evident also on the prospective of making more energy efficient buildings. This goal is achievable not only by using active systems [16] but also passive ones [17,18] and with the use of more eco-friendly material such as waste or secondary raw materials in construction [19–21]. In this research, the study of alternative binders of Ordinary Portland Cement (OPC) such as natural hydraulic lime (NHL) [22] and a partial substitution with by-products such as fly ash are of interest in order to obtain more sustainable materials for indoor application. In fact, in terms of materials, the cement industry represents one of the largest emitters of CO_2 [23]. While NHL is a more sustainable binder, due to the lower temperature required for its preparation, compared to that of cement, about 1000 °C instead of 1450 °C [24]. Another positive aspect related to the use of NHL in constructions is the high suitability of this product with the existing structure, and it can be used not only for new buildings but also for rehabilitation purposes of existing constructions [13].

With regard to the aggregates, the use of lightweight materials allows the production of lightweight mortars. Lightweight aggregates can have multiple origins: natural (pumice or vermiculite) or synthetic. In case of synthetic aggregates, they can be obtained by primary materials (e.g. expanded perlite or expanded clay) or by secondary raw materials (e.g. waste from expanded glass). Lightweight mortar brings superior properties to buildings where they are applied, e.g. a reduction of dead weight of the structure [25] with a consequent decrease in cost and increase in efficiency of the building. Also, the occupants of indoor spaces with lightweight mortars and renders can obtain advantages from the application of these materials, e.g. a lower thermal conductivity [26,27] and enhanced acoustic insulation acting as acoustic shielding [28]. The use of secondary raw materials is recommended instead of natural ones, mainly considering the good results in terms of mechanical resistance and thermal insulation obtained with expanded glass in non-cementitious binders [29]. In this study, the comparison of natural and synthetic aggregates based mortars is also performed.

The importance of pore structure in terms of pore diameters and pore size distribution and its influence on the macro properties of mortars is well known [30]. The efficiency of photocatalysis is enhanced with the increased content of micro-nanopores. It is confirmed that the best range of pores should be around 100 nm [13]. The correlation between the ranges of pores and photocatalytic activity has been investigated by Jimenez-Relinque et al. [31] who reported that the NO_x degradation performance is improved in the pore range of 0.5–0.05 μm. It is also shown that the microstructure influences the PCO capacity, in particular, a higher presence of macro-pores is related to a higher PCO efficiency. On the other hand, a high quantity of cementitious products would cover the catalyst [32]. This is an additional reason to test the efficiency of NHL, as it is very well known that the presence of hydration products is lower than that in cementitious-based mortars. The performance of aerial lime-based mortar with the addition of photocatalyst (TiO_2) was studied by Karatasios et al. [33]. The optimum percentage seems to be 6%. In the current study, it has been decided to apply lower amounts of TiO_2, 2% and 4% of the binder volume, based on the preliminary study. The increasing content of calcite over time could modify the PCO activity by modification of the pore size distribution [33]. Other studies demonstrated in cementitious mortar that a decrease in photoactivity was caused by carbonation. It has been observed that calcite grows on the surface of photocatalyst, consequently decreasing the photocatalytic efficiency [34]. NHL, with less amount of calcium oxide, could influence less the PCO activities. In case of indoor finishing mortar, it is also important to take into account that the presence of nano-sized materials changes not only the hardened state properties but also the fresh state properties [35].

The aim of this research is to develop an innovative product, able to fulfil the conventional requirements for finishing mortar material and, more importantly, to improve IAQ and comfort of occupants. This performance-based design takes into account the selection of raw materials, considering sustainability. Density and mechanical strength are tested following the relevant standards. Pore structure is studied with Brunauer – Emmett – Teller (BET) and Mercury Intrusion Porosimetry (MIP). Drying shrinkage and capillary water absorption are evaluated. IAQ enhancement is appreciated by thermal conductivity and photocatalytic efficiency. The relationships between the pore structure and other properties including capillary water absorption and air pollutant removal efficiency are analysed.

2. Experimental

2.1. Materials

The applied materials in this study are summarized in Table 1. With the particle density, it is possible to evaluate the volumetric substitution of binders and aggregates. The particle size distributions (PSDs) of aggregates are evaluated by mechanical sieving, while those of the powders are analysed with Laser Light Scattering (LLS) Mastersizer 2000. Fig. 1 shows the PSDs curves of the powders and aggregates used. The elemental compositions are determined by the XRF analysis (Table 2).

In this research, Portland cement CEM I 42.5 N class (CEM) is used as the reference binder (provided by ENCI, the Netherlands). The specific density of CEM is 3136 kg/m^3, evaluated using a gas pycnometer. The mineral phases of the cement are computed using Bogue method [36], as: C_3S 63.4%; C_2S 8.9%, C_3A 7.2% and C_4AF 10.0%. Natural Hydraulic Lime (NHL) is provided by KEIM (the Netherlands). This product belongs to NHL 3.5 according to UNI EN 459-1:2010. The C_2S content is about 21%. The specific density is measured by a gas pycnometer, 2537 kg/m^3. A commercial fly ash (FA) from coal combustion, Class F fly ash according to ASTM C 618 [37], is used, with a specific density of 2337 kg/m^3, evaluated using a gas pycnometer.

During research, two commercial lightweight aggregates are used. The first is a natural expanded silicate, ES (Rotocell®), with volcanic origins. The second is expanded glass, EG. EG comes from thermal treatment of waste from glass. For both types of lightweight aggregate, a letter from A (bigger size) to C (smaller size) is assigned depending on diameter. Expanded glass has round and more regular spheres than expanded silicates.

2.2. Mix design

From the original method developed by Andreasen and Andersen [38] for the best granulometric size distribution, Funk and Dinger [39] proposed a modified model, as:

$$P(D) = \frac{D^q - D^q_{min}}{D^q_{max} - D^q_{min}} \quad (1)$$

where P(D) is the fraction of total solid (binders, powders and aggregates) for the mixture; D_{min} and D_{max} are the minimum and the maximum diameter, respectively, in μm; q is distribution modulus.

Table 1
Specific densities of different materials.

Materials	Code	Specific density kg/m^3	Bulk density kg/m^3	Particle density kg/m^3
Cement CEM I 42.5 N	CEM	3136		
Fly Ash	FA	2337		
Natural Hydraulic Lime	NHL	2537		
ES 90–300	ES A		360	700
ES 0.25–0.5	ES B		320	700
ES 0.5–1	ES C		310	600
EG 0.1–0.3	EG A		450	800
EG 0.25–0.5	EG B		300	540
EG 0.5–1	EG C		250	450

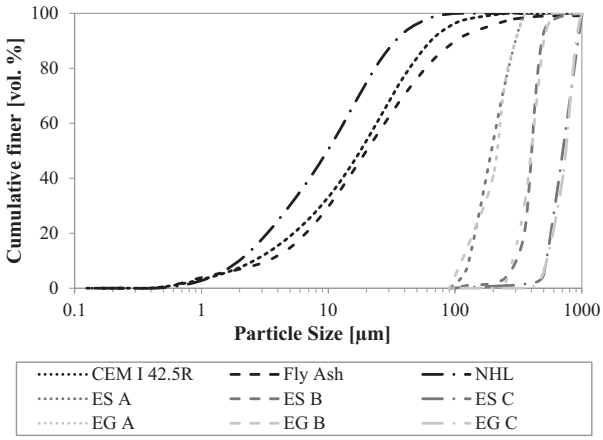

Fig. 1. PSDs curves of used binders and aggregates.

In this research, D_{max} of 1 mm is taken to prepare mortar finishing for indoor application as finish layer. The distribution modulus q is a variable and depends on the characteristics of the mixture, the chosen value is 0.5, following the suggestion of [40] which studied cement pastes with the addition of nano-materials. The total amount of different fractions is evaluated with an optimization algorithm based on Least Square Method (LSM) as proposed by [41,42]. A water to binder ratio of 1.6 by volume is used for all mixtures. Table 3 shows the compositions of the designed recipes.

The TiO_2 photocatalyst in the form of slurry is added to the mortars. The slurry is a commercial product (KRONOClean 7404), a carbon-doped titanium dispersed in water (40% of TiO_2 and 60% of water) with a pH of 7–8 and a density at 20 °C of about 1.4 g/cm^3. TiO_2 is substituted in two different quantities, as 2% and 4% of volume of binder. Zeolite is substituted during the preparation of mortars as 1 vol% of binder to improve the PCO reaction by enhancing the adsorption ability. Hashimoto et al. demonstrated that the titania-zeolite composite catalysts could enhance PCO activity [43]. In the presence of titania-zeolite composites, the adsorption data indicated the increase in the amount of NO adsorption on the TiO_2 phase and the decrease in the amount of NO_2 adsorption, compared to bare titania [43]. The BET specific surface area of zeolite is measured, 28.56 m^2/g. The same water to powder proportion based on volume is guaranteed by the subtraction of the water of the slurry. Table 3 shows the proportions of the mixes, with and without TiO_2.

2.3. Characterization of mortars

The workability is evaluated with the slump flow test according to the standard UNI EN 1015-3:2007 using a truncated cone (100 base diameter, 70 mm top diameter, and 60 mm height). The results are the mean of the two perpendicular diameters measured. The fresh density is determined by the ratio between the mass of the fresh mortar and the volume of samples (kg/m^3).

The densities are evaluated under two conditions: fresh state and oven dry conditions (according to UNI EN 1015-6:2007). The apparent density is measured by the size and mass of the sample. For hardened state conditions, the 40 × 40 × 160 mm^3 samples are cured for 28 days at T = (20 ± 2) °C and for the first 7 days at (95 ± 5)% RH and then for the following 21 days at (60 ± 5)% RH. After the curing period, specimens are placed inside an oven at (60 ± 2) °C until constant mass is reached. The flexural and compressive strengths of the sample at 28 days are determined according to the UNI EN 1015-11:2007 on three specimens for flexural and six specimens for compressive strengths.

The microstructure and porosity of mortar without TiO_2 additions are investigated with MIP (Thermo Fisher, Pascal series 240) and BET methods (Micrometics Tristar II). The pore size distribution is also investigated because some pore diameters are close to the dimension of nanoparticles that are applied in the mixes [44]. Both measurements are performed on samples after 28 days of curing, on three specimens and average values are used to interpret the results. The hydration of mortars is stopped by immersion and washing of specimens in ethanol. For the MIP analysis, fragments sampled for each mortar mix is about 1 cm^3 of volume. For the BET surface area and nano-porosity measurement, samples are extracted from the prepared mortar.

Concerning the fact that the mortars exposed to an environment with a relative humidity lower than (95 ± 5)% are subjected to shrinkage, the shrinkage behaviour is investigated under different conditions. Both the drying shrinkage and percentage of weight loss are evaluated and plotted with time on three specimens for each mix. The shrinkage is the measurement of the change in longitudinal dimension of specimens, in (mm/m). Eq. (2) is used to evaluate the percentage of weight loss (w_i):

Table 2
Chemical compositions (wt.%) of investigated powders.

	SiO_2	Al_2O_3	Fe_2O_3	CaO	MgO	K_2O	TiO_2	SO_3	P_2O_5	Others
CEM	19.64	4.80	3.28	63.34	1.99	0.56	0.34	2.87	0.59	1.03
FA	51.71	27.11	8.12	5.76	1.19	1.8	1.73	1.14	0.87	0.51
NHL	7.35	1.49	–	87.48	1.16	0.53	0.11	1.01	–	–
ZEO	75.11	13.26	2.18	3.87	0.58	4.63	0.28	0.06	–	0.05

Table 3
Composition of mixes (kg/m^3).

	CEM ES	CEM ES 2%	CEM ES 4%	CEM EG	CEM EG 2%	CEM EG 4%	NHL ES	NHL ES 2%	NHL ES 4%	NHL EG	NHL EG 2%	NHL EG 4%
w/b (by mass)	0.58	0.60	0.61	0.58	0.60	0.61	0.64	0.68	0.69	0.64	0.68	0.69
CEM	270.0	262.1	256.7	270.0	262.1	256.7	–	–	–	–	–	–
FA	201.0	195.3	191.3	201.0	195.3	191.3	201.0	195.3	191.3	201.0	195.3	191.3
NHL	–	–	–	–	–	–	219.0	212.0	207.6	219.0	212.0	207.6
Water	275.0	256.9	238.8	275.0	256.9	238.8	275.0	256.9	238.8	275.0	256.9	238.8
ES A	154.3	154.3	154.3	–	–	–	154.3	154.3	154.3	–	–	–
ES B	64.6	64.6	64.6	–	–	–	64.6	64.6	64.6	–	–	–
ES C	120.0	120.0	120.0	–	–	–	120.0	120.0	120.0	–	–	–
EG A	–	–	–	180.5	180.5	180.5	–	–	–	180.5	180.5	180.5
EG B	–	–	–	47.1	47.1	47.1	–	–	–	47.1	47.1	47.1
EG C	–	–	–	90.0	90.0	90.0	–	–	–	90.0	90.0	90.0
Slurry TiO_2	–	30.2	60.3	–	30.2	60.3	–	30.2	60.3	–	30.2	60.3
Zeolite	–	4.1	4.1	–	4.1	4.1	–	4.1	4.1	–	4.1	4.1

$$w_i = \frac{m_i - m_0}{m_0} \times 100[\%] \quad (2)$$

where m_i: weight at i-day in kg; m_0: weight at 24 h after the cast, in kg.

Water in porous materials can lead to the degradation of the durability of finishing. The absorbed capillary water affects all mortars in contact with the ground, in high humidity environments or exposed to atmospheric phenomena. Water can transport aggressive agents that can deteriorate the finishing [45]. Because of this reason, the study of water absorption is considered of primary importance to understand the durability of the investigated materials. The water absorption coefficient (C) due to the capillary action of the hardened mortar is evaluated according to UNI EN 1015-18:2004 on three specimens for each mix. The dry prismatic specimens with 40×40 mm^2 base area are weighed prior to immersion in water ranging from 5 to 10 mm. The weight is measured after 10 and 90 min of immersion, which is then used for the calculation of C. In order to explore the behaviour of mortar in terms of water absorption by capillary action in time, three specimens for each mix with 40×40 mm^2 base area are tested according to the standard UNI EN 15801:2010. Following this standard, the amount and rate at which a specimen absorbs water through the test surface when it is in contact with saturated filter paper is determined. The capillary water absorption is monitored and the amount of water absorbed by the specimen per unit area Q_i (kg/m^2) at time t_i ($s^{0.5}$) is calculated.

The influence of building materials on indoor microclimate is studied on two different aspects: one is referred to thermal properties, the other to the capacity of the mortar to decompose airborne harmful substances. The first aspect is addressed by the thermal conductivity of the specimens. Specimens of $100 \times 100 \times 100$ mm^3 are prepared. After a proper curing period (28 days), specimens are dried in a ventilated oven at (60 ± 3) °C until constant mass is reached. Then the specimens are cooled down at room temperature (T = 20 °C) and then the thermal conductivity of the specimens is measured with a heat analyser ISOMET 2104. Further tests are performed on samples after storing them in a humidity controlled chamber at (60 ± 5)% RH until constant mass is reached, in order to evaluate the influence of the humidity of the environment. For each condition, three tests are repeated on two specimens.

The plug-flow experimental setup used for the photocatalytic oxidation test is shown in Fig. 2. The used pollutant NO is mixed with synthetic air in order to reach the desired initial concentration. The concentration of pollutant and flow rate are chosen in order to represent realistic conditions. The tests are performed under two different radiation sources: UVA and visible light (VIS). Irradiation is provided with three fluorescent tubes emitting visible light and three emitting UVA light. For both cases, the light intensity is adjusted to about 10 W/m^2 and checked before each test. Two specimens for each mix prepared with 200×100 mm^2 surface area are tested. Measurements are performed at least two times. Temperature and humidity are kept constant at (22 ± 1) °C and (50 ± 2)% RH for all measurements. The pollutant concentration (NO, NO_x, NO_2) is measured by an online NOx analyser ANPA-370 (Horiba). Eq. (3) is used in order to determine the degradation ($NO_x deg$) of total NO_x ($NO + NO_2$):

$$NO_x deg = \frac{[C_{NO_x}]_{in} - [C_{NO_x}]_{out}}{[C_{NO_x}]_{in}} \times 100[\%] \quad (3)$$

where $[C_{NO_x}]_{in}$ is the initial concentration, in ppm; $[C_{NO_x}]_{out}$ is the outlet concentration; both values are the average between 5 min measurement, in ppm.

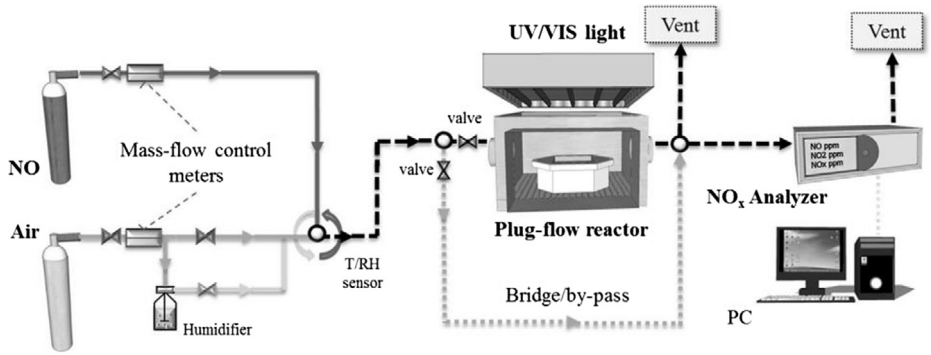

Fig. 2. Scheme of the plug-flow experimental setup [15].

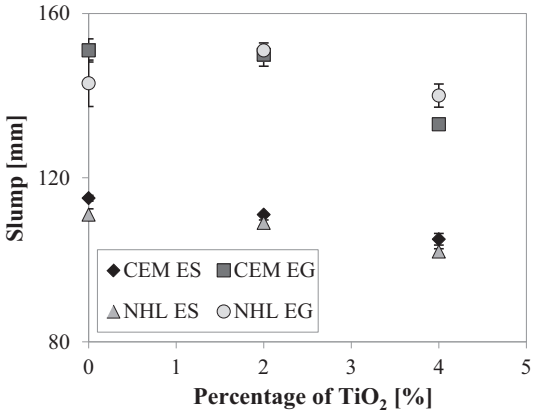

Fig. 3. Workability of mortars versus the dosage of photocatalyst.

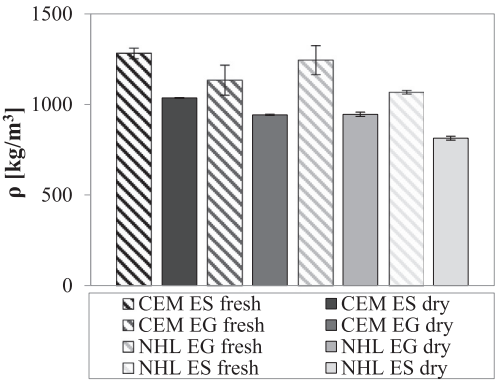

Fig. 4. Fresh state and oven dry density of mortars.

3. Results and discussions

3.1. Workability

All the mortars are prepared with the same amount of water and the same volumetric ratio between water to binder, so the fresh properties are influenced only by the aggregates, powders and TiO_2 content. When using the same aggregates, mortars have the same workability class: stiff with natural expanded silicates and plastic with expanded glass (classes according to UNI EN 1015-6:2007). This behaviour can be explained by the different particle shape of aggregates: spherical shape of expanded glass allows less friction forces between the aggregates that promote a better flow. Fig. 3 shows the different behaviour of mixes.

It is noted that when cement is substituted by NHL, slump values decrease. This is due to the finer particles present in NHL, as shown in Fig. 1, which need higher quantities of water to wet the surface. Concerning the mixes prepared with photocatalyst, it is observed that the same starting recipes have the same class of workability, except CEM EG 4% that turns from plastic to stiff. The presence of TiO_2 in general implies the loss of workability. TiO_2 has finer particles than other powders that can influence the workability especially by: a higher amount of water is needed to wet the surface while the particles exhibit high tendency to agglomerate due to strong cohesive van der Waals forces [35,46]. Obviously, a higher substitution of TiO_2 implies a higher loss of slump flow: the highest difference is recorded in cement-based mortar at 4% addition of TiO_2 with a decrease from 9% (with ES) to 12% (with EG). The difference is lower in NHL-based mortar, from 2% (with ES) to 8% (with EG).

It is also important to highlight that with these proportions no segregation is observed. In fact, one of the main problems in lightweight mortar or concrete is the lack of homogeneity: the very large differences between the densities of the used materials (binders and lightweight aggregates) may induce a static sedimentation of ingredients, causing segregation and loss of stability.

3.2. Density

Density is evaluated in both fresh and hardened states. As shown in Fig. 4, all mortars can be classified as lightweight mortars according to their oven dry density, less than 1300 kg/m^3, (as defined in UNI EN 998-1:2010). With the same binder, expanded glass based mixtures show lower density than the natural expanded silicate ones. With the same aggregate, NHL mortars have lower density than cement based mortar. The binder is also very influential in this study. In case of cement-based mortar, for 1 dm^3 of mix the mass loss of water during the oven dry process is about 24% for expanded silicate based mortar and 20% for expanded glass based mixtures. In case of NHL, the water loss is 31% for both mixtures. This obviously means that in the case of cement based mortar more water is used to form hydration products such as C-S-H gel.

3.3. Mechanical strength

Fig. 5 shows the development of flexural and compressive strengths during the curing period. As expected, cement based mortars have about three times higher flexural and compressive strength than NHL. NHL based mortars need at least 15 days to

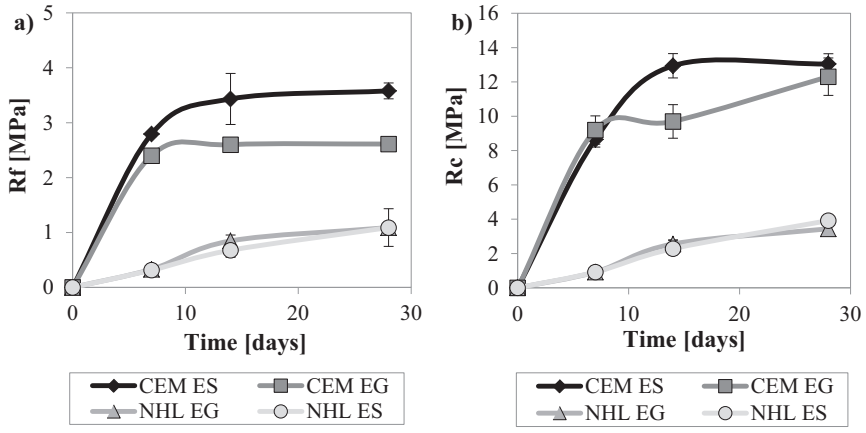

Fig. 5. Development of flexural (a) and compressive (b) strength of mortars at 7, 14 and 28 days.

have a compressive strength up to 2 MPa depending on the calcium hydroxide, $Ca(OH)_2$, content, as portlandite needs to be exposed to the environment to react with CO_2 to form $CaCO_3$, which has more mechanical resistance.

Thermogravimetric analysis (TGA) is performed on the NHL sample to assess the amount of portlandite. The results show two mass losses at two different temperatures: 5% at 450 °C and 25% at 650 °C, respectively. The mass loss at around 450 °C is attributed to the decomposition of $Ca(OH)_2$ [47], the percentage of total content of $Ca(OH)_2$ is calculated, yielding 21%. The mass loss at around 650 °C is due to the decarbonation of $CaCO_3$ [47], quantified as 57% of the total mass of NHL.

Over time, an increment of mechanical performance is also expected thanks to the positive interaction of FA with both binders. Nevertheless, for indoor finishing, a minimum compressive strength of 3 MPa should be acquired for indoor mortars [48] that is reached by all the different mixes. It is observed that in the case of lightweight mortar, the obtained density and strength relations are comparable with others found in literature, as shown in Fig. 6.

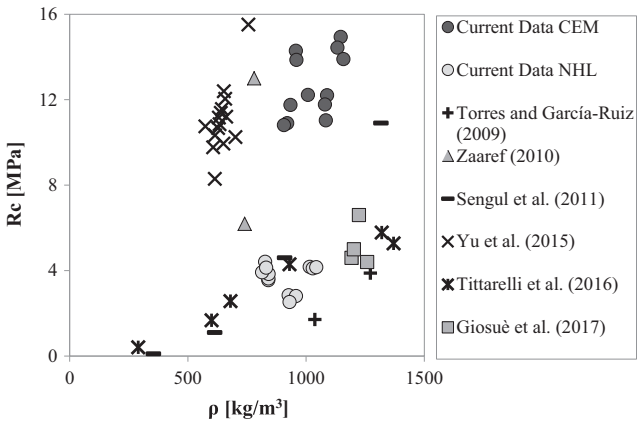

Fig. 6. Correlation between compressive strength and density. Current data and data from literature (Torres and García-Ruiz [49], Zaaref [50], Sengul et al. [51], Yu et al. [26], Tittarelli et al. [52], Giosuè et al. [53]).

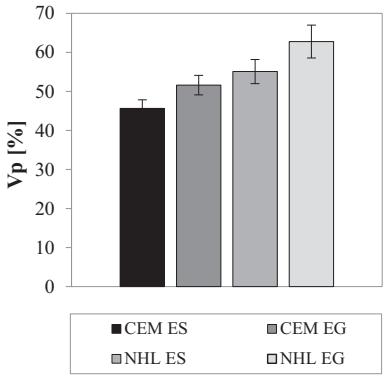

Fig. 7. Total amount of porosity of mortars evaluated with MIP analysis.

3.4. Pore structure

MIP analysis provides the total amount of open porosity and pore size distribution of mortars (Figs. 7 and 8). Table 4 summarizes the obtained results. Traditional cementitious mortars generally have about 15–19% lower values of accessible porosity (Vp) than that obtained in the current research [54,55]. The high values of Vp are mainly due to the intrinsic porosity of the aggregates and the high w/b ratio. When the same aggregate is used, different binders imply differences in the pore structure: the use of NHL instead of cement as a binder introduces a further 10% of total porosity. When the same binder is used, expanded glass introduces a further 5% of total porosity compared to expanded silicates. The use of NHL mortar, also owing to the pore structures of obtained finishing, could positively influence IAQ performance such as water vapour permeability [56] and moisture buffering capacity [57]. It has been reported that specimens with the highest transpiration capacity can possess the highest moisture buffer capacity [19] since the higher the porosity of mortars, the higher the moisture penetration depth [58].

Table 4 and Fig. 8 show the distributions of porosity of mortars. The main influential factor seems to be the type of binder, i.e. NHL induces a mortar with a higher quantity of pores at a higher diameter than cement-based mortar.

The BET analysis results are shown in Fig. 9. For the current ranges of pore size (2–200 nm), the results show that there are more pores with smaller diameters, corresponding to a higher amount of gel pores, in cement-based mortars than in NHL-based mortar. Several classifications of the pore system in a cementitious matrix have been defined. In the present research, the definition provided by Kumar and Bhattacharjee is considered: micro pores or gel pores have radius of 0.5–10 nm, mesopores or capillary pores have radius of 5 nm–5000 nm and macropores (mainly due to entrained air or inadequate compaction) have radius higher than 5000 nm [59]. Cement mortars present a higher amount of gel porosity than NHL since peaks are detected around diameter 10–

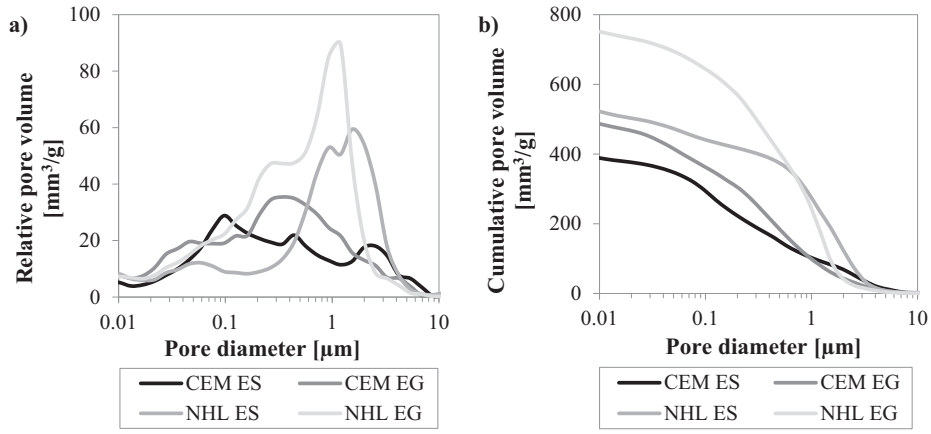

Fig. 8. Results from MIP analysis of mortars in terms of relative (a) and cumulative (b) pore distribution.

Table 4
MIP results: percentage of total open porosity and average pore diameter.

MIX	Total open porosity %	Average pore diameter μm
CEM ES	45.6	0.0866
CEM EG	51.6	0.0781
NHL ES	55.1	0.1104
NHL EG	62.8	0.1241

20 nm during the BET measurement (Fig. 9) instead of 100–200 nm of NHL.

3.5. Drying shrinkage

At the measurement time of 35 days, the values of shrinkage of the mortars are: 0.83 mm/m for CEM EG, 1.01 mm/m for CEM ES, 3.43 mm/m for NHL EG and 3.03 mm/m for NHL ES, respectively (Fig. 10).

In mortars, shrinkage depends mostly on aggregate/binder ratio. In this case, the volume of paste is equal in each mixture but the NHL-based mortars show higher values of shrinkage than that of cement-based ones. This difference is attributed to the different microstructure of mortars, since NHL mortars are more porous and the loss of mass due to water evaporation is higher. At the same aggregate/binder ratio, drying shrinkage depends on: open porosity, which facilitates water evaporation and pore distribution, because the finer the capillary network, the higher the capillary stress that generates shrinkage [54]. Fig. 11 shows the correlation between water loss and shrinkage and it is evident that for the same mass loss, the shrinkage of NHL mixes is higher than that for CEM mixes. This is due to the lower elastic modulus of NHL-based mortars as compared to cementitious ones as found in literature [60] which gives a higher shrinkage deformation at the same capillary stress due to water evaporation, because the lower the matrix stiffness, the higher the shrinkage generated at the same stress.

In NHL-based mortars, EG mortars shrink more than ES mortars because although they have comparable mechanical performances, water loss and probably elastic modulus, their higher porosity is shifted towards smaller pores that induces higher capillary stress at the same amount of evaporated water.

3.6. Capillary water absorption

Water absorption is influenced by pore structure. Water is absorbed at first in the macro pores and then it fills the capillary pores. The coefficient (Fig. 12a) is related to the first part of absorption once the bigger pores are filled. The types of binder and aggregate influence the porosity and consequently capillary water absorption [17].

NHL mortars present pores with higher diameters than CEM mortars, which explains the much higher values of the coefficient

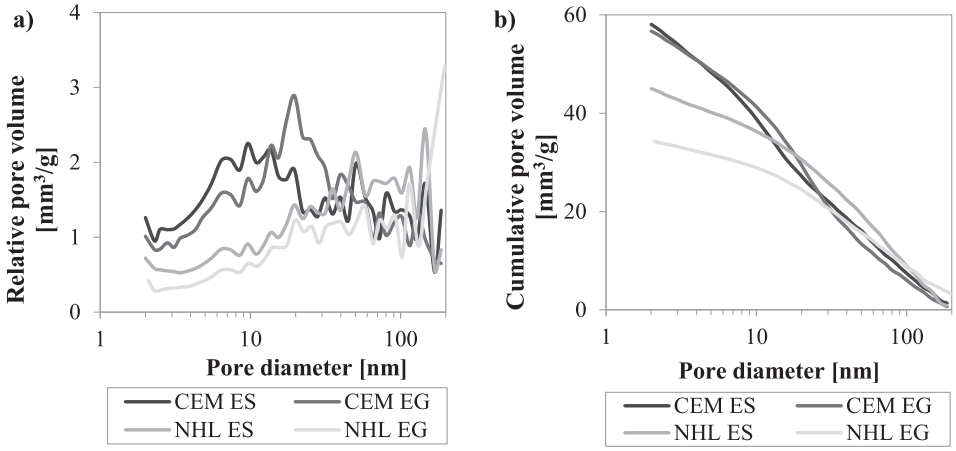

Fig. 9. Results from BET analysis of mortars in terms of relative (a) and cumulative (b) pore distribution.

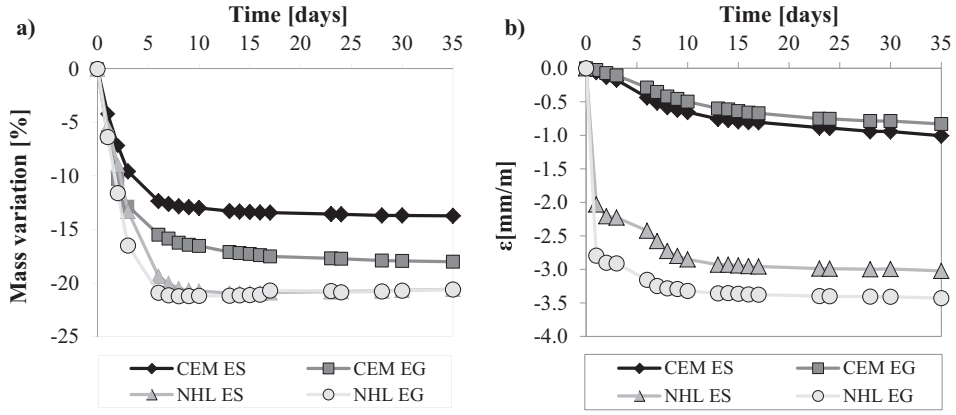

Fig. 10. Mass variation (a) and shrinkage (b) of mortar measured during 35 days.

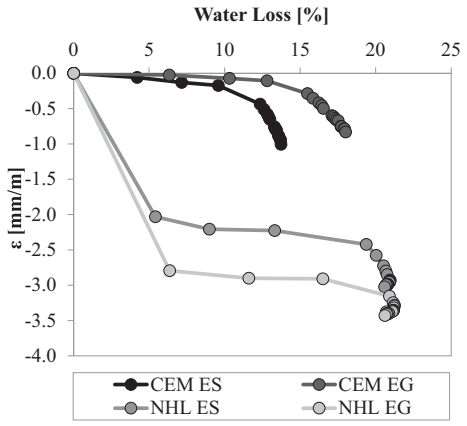

Fig. 11. Correlation between shrinkage and water loss of mortars.

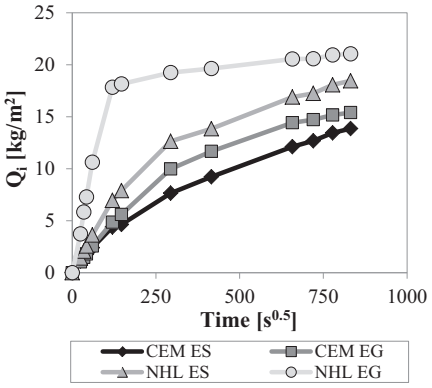

Fig. 13. Capillary water absorption development of mortars during the time.

in the case of NHL as binder. Another reason is the percentage of the accessible porosity, the higher the porosity, the higher the value of the coefficient [61], confirmed by the linear correlation shown in Fig. 12b. With regard to the aggregates, EG-based mortar has higher values of absorption coefficient compared to the natural ES used, which are hydrophobic aggregates as reported in the data sheet. The coefficient of CEM EG is higher than CEM ES by about 20%, when NHL is used, the coefficient is up to 35%.

The capillary water absorption is investigated not only in semi-immersion condition at a prefixed period of time (t = 90 min) but also over time (Fig. 13). With this method both the final amount of absorbed water and kinetics of water absorption can be evaluated. Concerning the total amount of absorbed water, it is well known that in porous media water absorption follows the law related to the Washburn equation [62]:

$$\Delta P = \frac{2\gamma \cos\theta}{r} \text{ [Pa]} \quad (4)$$

where γ is the surface tension of water, in Pa; θ is the contact angle; r is the radius of the pores.

NHL EG has the highest amount of porosity, 60%, consequently resulting in the highest amount of trapped water. In case of cement, the absorption of water is 15% higher in EG based samples than in ES lightweight aggregate based ones. This is due to the nature, shape and porosity of aggregates: expanded glass has a round shape, whereas expanded silicates due to their natural origin are more irregular in shape and have hydrophobic features, which introduces a high tortuosity of the water path [63].

Not only is the total open porosity important in terms of capillary absorption, but also its dimensional distribution. The kinetic curves can be divided in two phases: first linear and then non-linear. The first linear part of the water absorption curve corresponds to the filling of the bigger pores, the second non-linear phase to the filling of the smaller capillary pores, which are more frequent in cement mortars than in NHL ones, prolonging the time to reach stationary conditions. The hydrophobicity of the natural expanded silicates used influences the kinetics of water absorption: despite the higher amount of pores with bigger diameter compared to expanded glass, the stationary condition has not yet been reached at the end of the test.

3.7. Thermal properties

Thermal properties (Fig. 14) are evaluated at room temperature (T = 20 °C) on dry specimens and also on specimens that are pre-conditioned at 60% RH, in order to investigate the behaviour of mortars under a realistic indoor environment. As Fig. 14 shows, there are no relevant changes in thermal transmittance values apart from a slight increase in the variability of measurements when specimens are exposed at RH = 60%.

Due to similar results under these two conditions, only thermal conductivities under oven dry conditions are used for further analysis. CEM ES has the highest thermal conductivity. Compared to CEM ES, CEM EG has lower values of about 15%. Considering the NHL based mortar, NHL ES and NHL EG have 30% and 40% lower thermal conductivity values compared to CEM ES, respectively.

As expected, when the density increases, the thermal conductivity of mortars increases. There is a linear correlation between the dry density and thermal conductivity as shown in Fig. 15a, which is in line with [64]. Thermal conductivity is also proportional to the total porosity (Fig. 15b) [28]. The increase of porosity is related to the improvement of the thermal behaviour with a

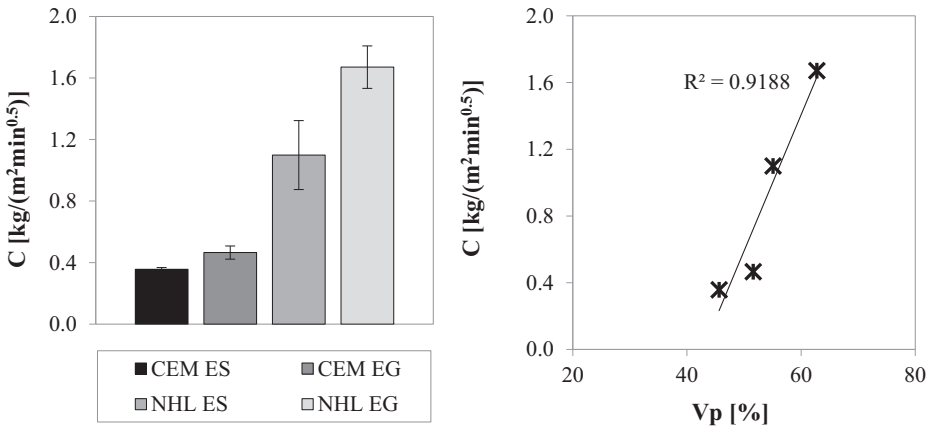

Fig. 12. (a) Capillary water absorption coefficient of mortars; (b) linear correlation between capillary water absorption coefficient and porosity.

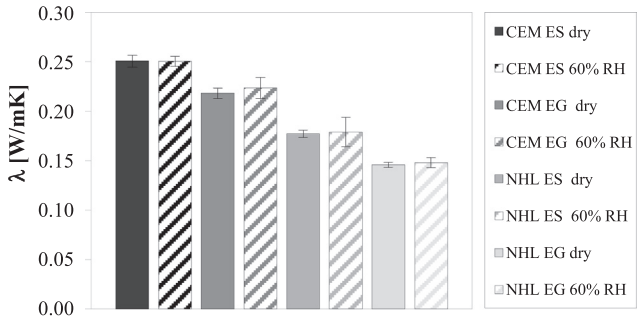

Fig. 14. Thermal conductivity of mortars.

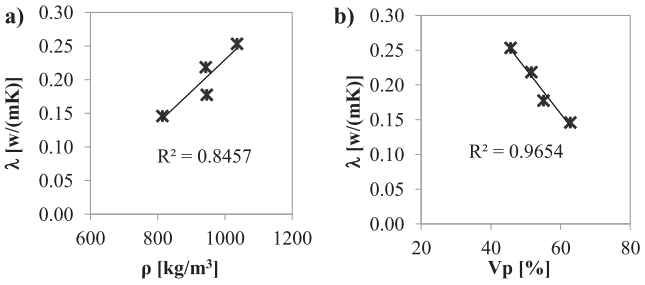

Fig. 15. Correlation between thermal conductivity and a) density, b) percentage of volume of pores.

lower thermal transmittance value. This behaviour is related to the porosity of the aggregate itself, in case of expanded glass the pores are not interconnected, which increases the thermal behaviour; in case of expanded silicates, the pores are more interconnected. The use of NHL can be related to an enhancement of indoor comfort of occupants, as these finishing contribute to thermal insulation.

3.8. Photocatalytic oxidation

The addition of TiO_2 enforces photocatalytic properties upon the mortar. The Langmuir Hinshelwood model has been used to interpret the reaction kinetics. Through the reactor a laminar flow is formulated with the applied volumetric air flow rate [12]. Fig. 16a plots the efficiency of the cement based samples under the UVA irradiation. It is evident that the higher the amount of TiO_2, the higher the PCO efficiency, and the increase of NO_x removal efficiency is 20% for both aggregates when the TiO_2 content is increased from 2% to 4%. It is observed that the use of expanded silicates instead of expanded glass ensures an increase in performance of about 15%.

The results obtained under visible (VIS) radiation (volumetric air low of 1.5 L/min and NO inlet concentration of 0.5 ppm) for cementitious mortars (Fig. 16b) show an obvious decrease in air purification efficiency, of about 65% for expanded silicates based mortar. The decrease is less for expanded glass cement mortar: in the case of mix containing 2% content of TiO_2 it is about 60% and in the case of 4% content of TiO_2 the efficiency is about 50% with respect to UVA radiation. With a double amount of TiO_2 in cement based mixtures there is an increase in PCO conversion rate of about 15% and 30% for expanded glass. In this case, expanded glass has a higher efficiency than expanded silicates based mortar under visible light irradiation. This aggregate seems to be more suitable for use under indoor illumination due to the high conversion rate. Expanded glass shows a higher workability than expanded silicates (Fig. 3) that can contribute to a better dispersion of TiO_2 in the matrix. So, the radiation can reach not only the superficial particles of the catalyst but also go deeper into the matrix. The difference between the behaviour and the material is more evident when the NHL based mortar is considered.

With respect to the cement based mortar, this finishing results in a lower efficiency, which is due to the higher presence of hydration product gel that can cover some of the active sites of titanium dioxide [65]. This is confirmed by the BET analysis: the higher the amount of gel pores, the lower the conversion rate (Fig. 17a).

The most effective depolluting mix is NHL and expanded glass based mortar with 4% of TiO_2 addition. The NO_x conversion rate of this mix is 80% higher than the 2% TiO_2 NHL expanded glass based mortar and 60% higher than cement expanded silicate based mortar with the same content of TiO_2 (4%). Taking into account that there is the same binder and the same TiO_2 content of NHL ES 4%, this behaviour could be related to the porosity of this mortar and it is not related to the reflectiveness of binder. NHL-EG mortar has a peak of high presence of porosity at about 1 μm diameter. This porosity is closer to [13], who stated that a nano-size porosity can decrease the depolluting capacity of the mortar even if the amount of TiO_2 is increased, as this pore size distribution and total porosity favours the pollutant access into the internal structure of the mortar. Indeed, the mortar with the highest conversion rate is NHL EG 4%, which has the highest value of average pore diameters evaluated by MIP analysis, which is confirmed by Fig. 17b. While a macro porosity is not useful to increase PCO capacity of mortar.

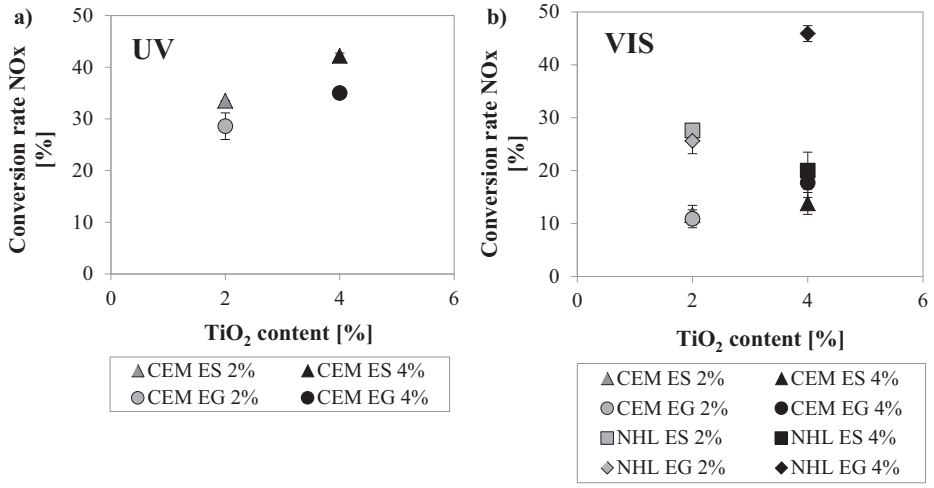

Fig. 16. Test results performed with a) UVA radiation, 3 L/min flux and 1 ppm pollutants and b) visible radiation, 1.5 L/min flux and 0.5 ppm pollutants.

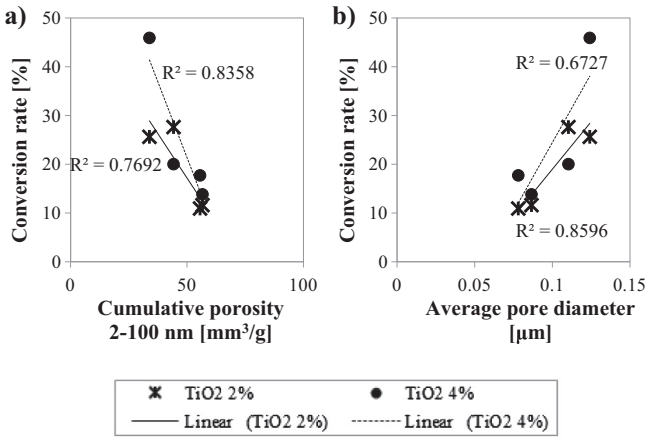

Fig. 17. Correlation between NOx conversion rate and a) cumulative pores from 2 to 100 nm evaluated by BET, and b) average pore diameter evaluated by MIP.

4. Conclusions

The present paper addresses photocatalytic lightweight indoor hydraulic lime-based finishing mortars, using Portland cement-based finishing mortar as a reference. Two different types of aggregates, expanded glass and expanded silicate, are utilized to achieve the lightweight character, and their effects on the performance are investigated. The porosity, pore structure, drying shrinkage, mechanical strength, thermal physical properties, and air pollutant removal ability of the developed finishing mortar are investigated. The relation between the pore structure and other mortar properties are studied. Based on the obtained results, the following consideration can be drawn:

- The expanded glass-based mortars have plastic workability, the expanded silicates are stiff. The presence of TiO_2 in general implies the loss of workability.
- The hydraulic lime-based mortars possess a higher capillary water absorption than cement-based mortar, due to the higher porosity. The expanded glass-based mortars show a higher capillary water absorption than expanded silicates mortar.
- The hydraulic lime-based mortars have a higher drying shrinkage than cement-based mortars, attributed to the Kelvin-Laplace mechanism. The expanded glass-based mortars show a higher shrinkage and absorption than expanded silicate due to the higher presence of smaller porosity.
- The hydraulic lime-based and expanded glass mortar shows very good thermal properties, with a low thermal conductivity of up to 0.15 W/(m·K), thanks to its high porosity.
- The hydraulic lime-based and expanded glass mortar show better air pollutant removal ability, up to 46% under indoor air conditions, compared to cement-based mortar, due to its lower content of gel pores.
- Both hydraulic lime and cement-based mortars, with expanded glass aggregates have a better ability to enhance the thermal insulation properties and air pollutant removal compared to expanded silicate aggregates.

References

[1] S. Wang, C. Yan, F. Xiao, Quantitative energy performance assessment methods for existing buildings, Energy Build. 55 (2012) 873–888, https://doi.org/10.1016/j.enbuild.2012.08.037.
[2] S.E. Frey, H. Destaillats, S. Cohn, S. Ahrentzen, M.P. Fraser, The effects of an energy efficiency retrofit on indoor air quality, Indoor Air. 25 (2015) 210–219, https://doi.org/10.1111/ina.12134.
[3] P. Blondeau, V. Iordache, O. Poupard, D. Genin, F. Allard, Relationship between outdoor and indoor air quality in eight French schools, Indoor Air. 15 (2005) 2–12, https://doi.org/10.1111/j.1600-0668.2004.00263.x.
[4] I. Ozga, N. Ghedini, C. Giosuè, C. Sabbioni, F. Tittarelli, A. Bonazza, Assessment of air pollutant sources in the deposit on monuments by multivariate analysis, Sci. Total Environ. 490 (2014), https://doi.org/10.1016/j.scitotenv.2014.05.084.
[5] A.H. Mamaghani, F. Haghighat, C.S. Lee, Photocatalytic oxidation technology for indoor environment air purification: the state-of-the-art, Appl. Catal. B Environ. 203 (2017) 247–269, https://doi.org/10.1016/j.apcatb.2016.10.037.
[6] A. Fujishima, X. Zhang, D.A. Tryk, TiO2 photocatalysis and related surface phenomena, Surf. Sci. Rep. 63 (2008) 515–582, https://doi.org/10.1016/j.surfrep.2008.10.001.
[7] D.E. MacPhee, A. Folli, Photocatalytic concretes – the interface between photocatalysis and cement chemistry, Cem. Concr. Res. 85 (2016) 48–54, https://doi.org/10.1016/j.cemconres.2016.03.007.
[8] Q.L. Yu, M.M. Ballari, H.J.H. Brouwers, Indoor air purification using heterogeneous photocatalytic oxidation. Part II: kinetic study, Appl. Catal. B Environ. 99 (2010) 58–65, https://doi.org/10.1016/j.apcatb.2010.05.032.
[9] J. Chen, C.S. Poon, Photocatalytic cementitious materials: influence of the microstructure of cement paste on photocatalytic pollution degradation, Environ. Sci. Technol. 43 (2009) 8948–8952, https://doi.org/10.1021/es902359s.
[10] S. Lorencik, Q.L. Yu, H.J.H. Brouwers, Photocatalytic coating for indoor air purification: synergetic effect of photocatalyst dosage and silica modification, Chem. Eng. J. 306 (2016) 942–952, https://doi.org/10.1016/j.cej.2016.07.093.
[11] J. Lim, P. Murugan, N. Lakshminarasimhan, J.Y. Kim, J.S. Lee, S.H. Lee, W. Choi, Synergic photocatalytic effects of nitrogen and niobium co-doping in TiO2 for the redox conversion of aquatic pollutants under visible light, J. Catal. 310 (2014) 91–99, https://doi.org/10.1016/j.jcat.2013.05.014.
[12] Q.L. Yu, H.J.H. Brouwers, Indoor air purification using heterogeneous photocatalytic oxidation. Part I: experimental study, Appl. Catal. B Environ. 92 (2009) 454–461, https://doi.org/10.1016/j.apcatb.2009.09.004.
[13] S.S. Lucas, V.M. Ferreira, J.L.B. De Aguiar, Incorporation of titanium dioxide nanoparticles in mortars — influence of microstructure in the hardened state properties and photocatalytic activity, Cem. Concr. Res. 43 (2013) 112–120, https://doi.org/10.1016/j.cemconres.2012.09.007.
[14] J. Vieira, L. Senff, H. Gonçalves, L. Silva, V.M. Ferreira, J.A. Labrincha, Functionalization of mortars for controlling the indoor ambient of buildings, Energy Build. 70 (2014) 224–236, https://doi.org/10.1016/j.enbuild.2013.11.064.
[15] S. Lorencik, Q.L. Yu, H.J.H. Brouwers, Design and performance evaluation of the functional coating for air purification under indoor conditions, Appl. Catal. B Environ. 168–169 (2015) 77–86, https://doi.org/10.1016/j.apcatb.2014.12.012.
[16] M. Pierpaoli, C. Giosuè, M.L. Ruello, G. Fava, Appraisal of a hybrid air cleaning process, Environ. Sci. Pollut. Res. 24 (2017) 12638–12645, https://doi.org/10.1007/s11356-016-7880-x.
[17] F. Tittarelli, C. Giosuè, A. Mobili, M.L. Ruello, Influence of binders and aggregates on VOCs adsorption and moisture buffering activity of mortars for indoor applications, Cem. Concr. Compos. 57 (2015), https://doi.org/10.1016/j.cemconcomp.2014.11.013.
[18] O.F. Osanyintola, C.J. Simonson, Moisture buffering capacity of hygroscopic building materials: experimental facilities and energy impact, Energy Build. 38 (2006) 1270–1282, https://doi.org/10.1016/j.enbuild.2006.03.026.
[19] C. Giosuè, A. Mobili, G. Toscano, M.L. Ruello, F. Tittarelli, Effect of biomass waste materials as unconventional aggregates in multifunctional mortars for indoor application, Procedia Eng. 161 (2016) 655–659, https://doi.org/10.1016/j.proeng.2016.08.724.
[20] V. Sata, J. Tangpagasit, C. Jaturapitakkul, P. Chindaprasirt, Effect of W/B ratios on pozzolanic reaction of biomass ashes in Portland cement matrix, Cem. Concr. Compos. 34 (2012) 94–100, https://doi.org/10.1016/j.cemconcomp.2011.09.003.
[21] R.V. Silva, J. de Brito, R.K. Dhir, Performance of cementitious renderings and masonry mortars containing recycled aggregates from construction and demolition wastes, Constr. Build. Mater. 105 (2016) 400–415, https://doi.org/10.1016/j.conbuildmat.2015.12.171.
[22] M.M. Ballari, Q.L. Yu, H.J.H. Brouwers, Experimental study of the NO and NO2 degradation by photocatalytically active concrete, Catal. Today 161 (2011) 175–180, https://doi.org/10.1016/j.cattod.2010.09.028.
[23] L. Barcelo, J. Kline, G. Walenta, E. Gartner, Cement and carbon emissions, Mater. Struct. 47 (2013) 1055–1065, https://doi.org/10.1617/s11527-013-0114-5.
[24] J. Válek, E. Van Halem, A. Viani, M. Pérez-Estébanez, R. Ševčík, P. Šašek, Determination of optimal burning temperature ranges for production of natural hydraulic limes, Constr. Build. Mater. 66 (2014) 771–780, https://doi.org/10.1016/j.conbuildmat.2014.06.015.
[25] A. Kiliç, C.D. Atiş, E. Yaşar, F. Özcan, High-strength lightweight concrete made with scoria aggregate containing mineral admixtures, Cem. Concr. Res. 33 (2003) 1595–1599, https://doi.org/10.1016/S0008-8846(03)00131-5.
[26] Q.L. Yu, P. Spiesz, H.J.H. Brouwers, Ultra-lightweight concrete: conceptual design and performance evaluation, Cem. Concr. Compos. 61 (2015) 18–28, https://doi.org/10.1016/j.cemconcomp.2015.04.012.
[27] J. Kurnitski, T. Kalamees, J. Palonen, L. Eskola, O. Seppänen, Potential effects of permeable and hygroscopic lightweight structures on thermal comfort and perceived IAQ in a cold climate, Indoor Air. 17 (2007) 37–49, https://doi.org/10.1111/j.1600-0668.2006.00447.x.

[28] H.K. Kim, J.H. Jeon, H.K. Lee, Workability, and mechanical, acoustic and thermal properties of lightweight aggregate concrete with a high volume of entrained air, Constr. Build. Mater. 29 (2012) 193–200, https://doi.org/10.1016/j.conbuildmat.2011.08.067.
[29] D.M.A. Huiskes, A. Keulen, Q.L. Yu, H.J.H. Brouwers, Design and performance evaluation of ultra-lightweight geopolymer concrete, Mater. Des. 89 (2016) 516–526, https://doi.org/10.1016/j.matdes.2015.09.167.
[30] S. Care, F. Derkx, Determination of relevant parameters influencing gas permeability of mortars, Constr. Build. Mater. 25 (2011) 1248–1256, https://doi.org/10.1016/j.conbuildmat.2010.09.028.
[31] E. Jimenez-Relinque, J.R. Rodriguez-Garcia, A. Castillo, M. Castellote, Characteristics and efficiency of photocatalytic cementitious materials: Type of binder, roughness and microstructure, Cem. Concr. Res. 71 (2015) 124–131, https://doi.org/10.1016/j.cemconres.2015.02.003.
[32] R. Sugrañez, J.I. Álvarez, M. Cruz-yusta, I. Mármol, J. Morales, J. Vila, L. Sánchez, Enhanced photocatalytic degradation of NOx gases by regulating the microstructure of mortar cement modified with titanium dioxide, Build. Environ. 69 (2013) 55–63, https://doi.org/10.1016/j.buildenv.2013.07.014.
[33] I. Karatasios, M.S. Katsiotis, V. Likodimos, A.I. Kontos, G. Papavassiliou, P. Falaras, V. Kilikoglou, Photo-induced carbonation of lime-TiO2 mortars, Appl. Catal. B Environ. 95 (2010) 78–86, https://doi.org/10.1016/j.apcatb.2009.12.011.
[34] M.V. Diamanti, F. Lollini, M.P. Pedeferri, L. Bertolini, Mutual interactions between carbonation and titanium dioxide photoactivity in concrete, Build. Environ. 62 (2013) 174–181, https://doi.org/10.1016/j.buildenv.2013.01.023.
[35] L. Senff, D.M. Tobaldi, S. Lucas, D. Hotza, V.M. Ferreira, J.A. Labrincha, Formulation of mortars with nano-SiO2 and nano-TiO2 for degradation of pollutants in buildings, Compos. Part B 44 (2013) 40–47, https://doi.org/10.1016/j.compositesb.2012.07.022.
[36] A.M. Neville, Properties of Concrete, Longman, London, UK, 1995.
[37] X. Gao, Q.L. Yu, H.J.H. Brouwers, Reaction kinetics, gel character and strength of ambient temperature cured alkali activated slag-fly ash blends, Constr. Build. Mater. 80 (2015) 105–115, https://doi.org/10.1016/j.conbuildmat.2015.01.065.
[38] A.H.M. Andreasen, A. J., Ueber die Beziehung zwischen Kornabstufung und Zwischenraum in Produkten aus losen Kornern (mit einigen Experimenten), Kolloid-Zeitschrift. 50 (1930) 217–228. doi:10.1007/BF01422986.
[39] J.E. Funk, D.R. Dinger, Predictive Process Control of Crowded Particulate Suspensions: Applied to Ceramic Manufacturing, Kluwer Academic, USA, 1994.
[40] G. Quercia, G. Hüsken, H.J.H. Brouwers, Water demand of amorphous nano silica and its impact on the workability of cement paste, Cem. Concr. Res. 42 (2012) 344–357, https://doi.org/10.1016/j.cemconres.2011.10.008.
[41] Q.L. Yu, Design of Environmentally Friendly Calcium Sulfate-Based Building Materials. Towards and Improved Indoor Air Quality PhD thesis., Eindhoven University of Technology, Eindhoven, Netherlands, 2012.
[42] G. Hüsken, A Multifunctional Design Approach for Sustainable Concrete with Application to Concrete Mass Products PhD thesis, Eindhoven University of Technology, Eindhoven, Netherlands, 2010.
[43] K. Hashimoto, K. Wasada, M. Osaki, E. Shono, K. Adachi, N. Toukai, H. Kominami, Y. Kera, Photocatalytic oxidation of nitrogen oxide over titania – zeolite composite catalyst to remove nitrogen oxides in the atmosphere, Appl. Catal. B Environ. 30 (2001) 429–436, https://doi.org/10.1016/S0926-3373(00)00258-7.
[44] T. Fen-Chong, K. Li, P. Dangla, Q. Zeng, Pore structure of cement pastes through NAD and MIP analysis, Adv. Cem. Res. 28 (2015) 23–32, https://doi.org/10.1680/adcr.14.00109.
[45] V. Corinaldesi, G. Moriconi, F. Tittarelli, Thaumasite: Evidence for incorrect intervention in masonry restoration, Cem. Concr. Compos. 25 (2003) 1157–1160, https://doi.org/10.1016/S0958-9465(03)00158-6.
[46] R. Zhang, X. Cheng, P. Hou, Z. Ye, Influences of nano-TiO2 on the properties of cement-based materials: hydration and drying shrinkage, Constr. Build. Mater. 81 (2015) 35–41, https://doi.org/10.1016/j.conbuildmat.2015.02.003.
[47] M. Arandigoyen, J.L. Pérez, Bernal, M.A. Bello Lopez, J.I. Alvarez, Lime-pastes with different kneading water: pore structure and capillary porosity, Appl. Surf. Sci. 252 (2005) 1449–1459, https://doi.org/10.1016/j.apsusc.2005.02.145.
[48] M. Theodoridou, L. Kyriakou, I. Ioannou, PCM-enhanced lime plasters for vernacular and contemporary architecture, Energy Procedia. 97 (2016) 539–545, https://doi.org/10.1016/j.egypro.2016.10.070.
[49] M.L. Torres, P.A. García-Ruiz, Lightweight pozzolanic materials used in mortars: evaluation of their influence on density, mechanical strength and water absorption, Cem. Concr. Compos. 31 (2009) 114–119, https://doi.org/10.1016/j.cemconcomp.2008.11.003.
[50] M.E. Zareef, Conceptual and Structural Design of Buildings Made of Lightweight and Infra – Lightweight Concrete PhD Tesis, Techn. Univ, Berlin, German, 2010.
[51] O. Sengul, S. Azizi, F. Karaosmanoglu, M.A. Tasdemir, Effect of expanded perlite on the mechanical properties and thermal conductivity of lightweight concrete, Energy Build. 43 (2011) 671–676, https://doi.org/10.1016/j.enbuild.2010.11.008.
[52] F. Tittarelli, C. Giosuè, A. Mobili, C. di Perna, S. Monosi, Effect of using recycled instead of virgin EPS in lightweight mortars, Procedia Eng. 161 (2016) 660–665, https://doi.org/10.1016/j.proeng.2016.08.728.
[53] C. Giosuè, M. Pierpaoli, A. Mobili, M.L. Ruello, F. Tittarelli, Influence of binders and lightweight aggregates on the properties of cementitious mortars: from traditional requirements to indoor air quality improvement, Materials (Basel). 10 (2017) 978, https://doi.org/10.3390/ma10080978.
[54] P. Chindaprasirt, S. Rukzon, Strength, porosity and corrosion resistance of ternary blend Portland cement, rice husk ash and fly ash mortar, Constr. Build. Mater. 22 (2008) 1601–1606, https://doi.org/10.1016/j.conbuildmat.2007.06.010.
[55] A. Mobili, A. Belli, C. Giosuè, T. Bellezze, F. Tittarelli, Metakaolin and fly ash alkali-activated mortars compared with cementitious mortars at the same strength class, Cem. Concr. Res. 88 (2016), https://doi.org/10.1016/j.cemconres.2016.07.004.
[56] B. Mazhoud, F. Collet, S. Pretot, J. Chamoin, Hygric and thermal properties of hemp-lime plasters, Build. Environ. 96 (2016) 206–216, https://doi.org/10.1016/j.buildenv.2015.11.013.
[57] H. Gonçalves, B. Gonçalves, L. Silva, F. Raupp-Pereira, L. Senff, J.A. Labrincha, Development of porogene-containing mortars for levelling the indoor ambient moisture, Ceram. Int. 40 (2014) 15489–15495, https://doi.org/10.1016/j.ceramint.2014.07.010.
[58] E. Latif, M. Lawrence, A. Shea, P. Walker, Moisture buffer potential of experimental wall assemblies incorporating formulated hemp-lime, Build. Environ. 93 (2015) 199–209, https://doi.org/10.1016/j.buildenv.2015.07.011.
[59] R. Kumar, B. Bhattacharjee, Porosity, pore size distribution and in-situ strength of concrete, Cem. Concr. Res. 33 (2003) 155–164, https://doi.org/10.1016/S0008-8846(02)00942-0.
[60] A. Kalagri, I. Karatasios, V. Kilikoglou, The effect of aggregate size and type of binder on microstructure and mechanical properties of NHL mortars, Constr. Build. Mater. 53 (2014) 467–474, https://doi.org/10.1016/j.conbuildmat.2013.11.111.
[61] F. Tittarelli, Effect of low dosages of waste GRP dust on fresh and hardened properties of mortars: Part 2, Constr. Build. Mater. 47 (2013) 1539–1543, https://doi.org/10.1016/j.conbuildmat.2013.06.086.
[62] E.W. Washburn, Note on a method of determining the distribution of pore sizes in a porous material, Proc. Natl. Acad. Sci. U. S. A. 7 (1921) 115–116, https://doi.org/10.1073/pnas.7.4.115.
[63] F. Tittarelli, S.P. Shah, Effect of low dosages of waste GRP dust on fresh and hardened properties of mortars: Part 1, Constr. Build. Mater. 47 (2013) 1532–1538, https://doi.org/10.1016/j.conbuildmat.2013.06.086.
[64] M.M. Barbero-Barrera, A. García-Santos, F.J. Neila-González, Thermal conductivity of lime mortars and calcined diatoms. Parameters influencing their performance and comparison with the traditional lime and mortars containing crushed marble used as renders, Energy Build. 76 (2014) 422–428, https://doi.org/10.1016/j.enbuild.2014.02.065.
[65] J. Chen, S.C. Kou, C.S. Poon, Photocatalytic cement-based materials: comparison of nitrogen oxides and toluene removal potentials and evaluation of self-cleaning performance, Build. Environ. 46 (2011) 1827–1833, https://doi.org/10.1016/j.buildenv.2011.03.004.